Fitting Cylinders Computation with an Application to Measuring $3D$ Shapes

Joviša Žunić * and Padraig Corcoran †

Abstract

This paper observes a fitting cylinders problem for $3D$ shapes. The method presented defines two cylinders that fit well with the shape considered. These cylinders are easy and fast to compute. Would the $3D$ shape considered be digitized, i.e. represented by the set of voxels, the computation is asymptotically optimal. Precisely, the time required for the computation is $\mathcal{O}(N)$, where N is the number of voxels inside the shape.

Next, we show how these fitting cylinders can be used to measure $3D$ shapes. More precisely, we define a new $3D$ shape measure that numerically evaluates how mach a shape given looks like a cylinder. Interestingly, both fitting cylinders have to be used to define such a measure - just one of them is not sufficient. The new measure is invariant with respect to translation, rotation, and scaling transformations, and ranges over the interval $[0; 1]$, and takes the value 1 if and only if the shape considered is a perfect cylinder. It is robust and simple to compute.

Key-words: Fitting $3D$ shapes, fitting objects by cylinders, $3D$ moments, invariants, object fitting efficiency, $3D$ shape measure.

1 Introduction

This paper deals with shape fitting and shape measurement problems - two recurrent problems in pattern recognition, image processing, and computer vision. More precisely, we deal with fitting cylinders and cylinderness measure for $3D$ shapes. Being one of the basic shapes that appear frequently in different domains, from medicine to the industry, a spectrum of the problems related

*Mathematical Institute, Serbian Academy of Sciences, Belgrade.
e-mail: jovisa_zunic@mi.sanu.ac.rs
†School of Computer Science and Informatics, Cardiff University, U.K.
e-mail: CorcoranP@cardiff.ac.uk

to cylindrical shapes were already studied in the literature. Just to mention the cylindrical surface fitting problems, [22, 23, 30, 32], segmentation problem [17], parameters estimation problem [7], or the registration problem [2], for an illustration.

The research related to the $3D$ shape based object analysis was not so intensive at the beginning of a usage of computers for manipulation and processing of image based data. It becomes more important due to the developments in the $3D$ image technologies, and a $3D$ data availability. Initially, the shape characterization based on the $3D$ moment invariants has been done – [14, 16, 28]. A study on an analogue of the famous Hu moment invariants [12, 16] that has resulted in designing a compactness measure [36] for $3D$ shapes, and latter on recovering ellipsoidness measures [15, 35], is another set of problems that have been considered. The cubeness [19], vesselness [8], rectilinearity [13], Minkowski compactness measure [18], are other examples of the numerical characterizations of the $3D$ shapes.

So far, most shape measures are developed related to a study of two-dimensional shape properties. Most popular shape properties have allocated multiple shape measures. Just to mention two of them, ellipticity [1, 21, 29, 38] and circularity [10, 24, 34]. Of course, there are many more shape properties that have been evaluated numerically: squareness [27], elongation [33, 37], anisotropy [25], bizarreness [3], and so on. There are also measures particularly related to the curve properties [9], curve temperature [6], linearity [26], and many more.

In this paper we introduce a new $3D$ shape measure, herein named *shape cylinderness measure*. This is a global shape descriptor, in sense that all the shape points are used for the computation – not only the boundary ones. The $3D$ shape cylinderness measure evaluates how much the object considered looks like a cylinder. The new measure ranges over the interval $[0, 1]$, takes the value 1 if and only if the shape measured is a cylinder. Also, it is invariant with respect to the translations, rotations, and scaling transformations. In addition, the new measure is simple to compute and is robust.

The paper is organized as follows: The next section includes the basic notations and definitions used in the paper. Section 3 establishes a theoretical framework for the definition of the new fitting cylinders, for $3D$ shapes. It has turned out that our method leads to two fitting cylinders, for a given $3D$ shape, for a small exception for almost spherical shapes. The computation is efficient, and would voxlized data are used is asymptotically optimal.

In the Section 4, we use these fitting cylinders to design a new $3D$ shape measure, numerical evaluation how much a given set looks like a cylinder[1]. A formal definition of the new measure is given there, as well.

Experimental illustrations are in the Section 5. The same section includes a modification of the cylinderness measure from the Section 4. Such a modification enables a simpler computation.

[1]Here in, by *a cylinder* we mean a $3D$ body, not a cylindrical surface.

Concluding remarks are in the last section.

2 Notations and Definitions

We start with the basic notations and definitions, used in this paper.

- So called, *geometric moments*, $m_{p,q}(S)$, of a $3D$ region/shape S are defined as follows

$$m_{p,q,r}(S) \;=\; \iiint_S x^p y^q z^r dxdydz. \tag{1}$$

- The moments $m_{0,0,0}(S)$, $m_{1,0,0}(S)$, $m_{0,1,0}(S)$, and $m_{0,0,1}(S)$ are used to define the shape centroid, $(x_c(S), y_c(S), z_c(S))$, formally defined as

$$\begin{aligned} (x_c(S), y_c(S), z_c(S)) \;=& \\ \left(\frac{m_{1,0,0}(S)}{m_{0,0,0}(S)}, \frac{m_{0,1,0}(S)}{m_{0,0,0}(S)}, \frac{m_{0,0,1}(S)}{m_{0,0,0}(S)}\right) & \end{aligned} \tag{2}$$

  Obviously, if the shape in question is assumed to be of a unit volume, i.e. $m_{0,0,0}(S) = 1$, then the point $(m_{1,0,0}(S),\ m_{0,1,0}(S),\ m_{0,0,1}(S))$ coincides with the centroid o S.

- To simplify theoretical derivations and without loss of generality, we will assume that all the shapes considered will be translated such that their centroid coincides with the origin. Thus,

$$(x_c(S), y_c(S), z_c(S)) \;=\; (0, 0, 0) \tag{3}$$

  would be assumed even though has not been mentioned.

- In our derivations we will use a well known quantity, $J(S)$ [16], defined as

$$J(S) = \frac{m_{2,0,0}(S) + m_{0,2,0}(S) + m_{0,0,2}(S)}{m_{0,0,0}(S)^{5/3}}, \tag{4}$$

  assuming that the centroid of S and the origin coincide. $J(S)$ is invariant with respect to translations, rotations, and scaling transformations. Actually, $J(S)$ might be seen as a $3D$ analogue of the first Hu moment shape invariant [12], commonly used in shape based object analysis tasks.

- By a *cylinder* $C(h, a)$ we mean a $3D$ body bounded by the two hyper-planes z_1 and z_2, and a circular oval w – all three cylinder bounding surfaces are defined as follows (for an illustration see Fig.1):

$$\begin{aligned} z_1 &= \left\{(x, y, z) | z = \frac{h}{2}\right\}, \\ z_2 &= \left\{(x, y, z) | z = -\frac{h}{2}\right\}, \\ w &= \left\{(x, y, z) | x^2 + y^2 = a^2\right\}. \end{aligned} \tag{5}$$

In other words,

$$C(h,a) = \left\{ (x,y,z) \mid |z| \leq \frac{h}{2},\ x^2+y^2 \leq a^2 \right\}. \tag{6}$$

If the cylinder $C(h,a)$ has the volume equal to 1, then $a = \frac{1}{\sqrt{\pi \cdot h}}$. In other words, $C(h,a)$ is dependent on a single parameter h. For a shorten denotation we will write $C(h)$, instead of $C(h,a)$. Thus,

$$C(h) \ = \ C(h,a) \ = \ C\left(h, a = \frac{1}{\sqrt{\pi \cdot h}}\right). \tag{7}$$

The parameters h and a would be called the *height* and *base radius*, of the cylinder $C(h,a)$, respectively.

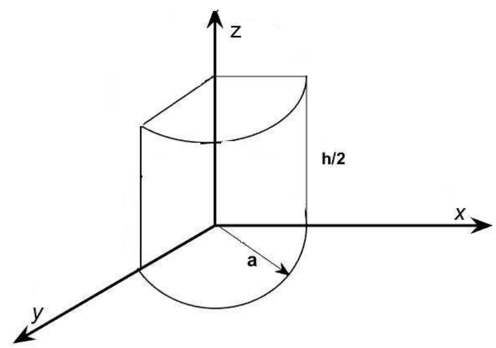

Figure 1: A part of a cylinder, from the first octant, positioned as defined by their surface equations given as in (5).

3 Fitting Cylinders for $3D$ Shapes

In this section, first we develop a theoretical framework needed to compute two fitting cylinders, for a given $3D$ shape. A formal definition for these two cylinders follows easily from the theoretical observations made. Experimental illustrations are in a separate subsection.

We start from the formulas for the volume $Vol(C(a,h))$ of the cylinder $C(a,h)$ and for the invariant $J(C(a,h))$ (as given in (4)). These are as follows:

$$\begin{aligned} Vol(C(h,a)) &= \pi \cdot a^2 \cdot h, \\ J(C(h,a)) &= \frac{1}{(\pi \cdot h \cdot a^2)^{2/3}} \cdot \left(\frac{h^2}{12} + \frac{a^2}{2} \right). \end{aligned} \tag{8}$$

The expression for $Vol(C(a,h))$ is trivial, while a derivation of expression for $J(C(h,a))$ follows

$$\begin{aligned}
& J(C(h,a)) = \\
= & \frac{1}{(\pi \cdot h \cdot a^2)^{5/3}} \cdot \iiint_{C(a,h)} (x^2+y^2+z^2) dxdydz & (9)\\
= & \frac{1}{(\pi \cdot h \cdot a^2)^{5/3}} \int_0^{2\pi}\int_0^a\int_{-h/2}^{h_2} \left(\rho^3+\rho z^2\right) d\phi d\rho dz & (10)\\
= & \frac{2\cdot\pi}{(\pi \cdot h \cdot a^2)^{5/3}} \cdot \int_0^a\int_{-h/2}^{h/2} \left(\rho^3+\rho z^2\right) d\rho dz & (11)\\
= & \frac{2\cdot\pi}{(\pi \cdot h \cdot a^2)^{5/3}} \cdot \int_0^a \left(h\rho^3+\frac{\rho}{12}h^3\right) d\rho & (12)\\
= & \frac{\pi\cdot h\cdot a^2}{(\pi \cdot h \cdot a^2)^{5/3}} \cdot \left(\frac{h^2}{12}+\frac{a^2}{2}\right) & (13)\\
= & \frac{1}{(\pi \cdot h \cdot a^2)^{2/3}} \cdot \left(\frac{h^2}{12}+\frac{a^2}{2}\right). & (14)
\end{aligned}$$

If we set the volume of $C(h,a)$ to be equal to 1, we have the following two equivalent equalities, satisfied by $J(C(h,a))$

$$\begin{aligned}
J\left(C\left(h=\frac{1}{\pi\cdot a^2},a\right)\right) &= \frac{a^2}{2}+\frac{1}{12\cdot\pi^2\cdot a^4},\\
J\left(C\left(h,a=\frac{1}{\sqrt{\pi\cdot h}}\right)\right) &= \frac{1}{2\cdot\pi\cdot h}+\frac{h^2}{12}.
\end{aligned} \tag{15}$$

We will exploit the second equality from (15), and use the notations from (7), to receive the following equality satisfied by h. form:

$$\pi\cdot h^3 - 12\cdot\pi\cdot J(C(h,a))\cdot h+6 = 0. \tag{16}$$

$3D$ shape moment invariant $J(S)$ is a distinct and natural $3D$ shape characteristic. Looking at the formula in (4), it can be concluded (for more details see [35, 36]) that $J(S)$ evaluates the average squared distance of the points from S to the centroid of S. As such, the quantity $J(S)$ is invariant with respect to the translations, rotations, and scaling transformations. Thus, a use of isometric transformations, to place the objects compared into a desirable position, is not necessary. This is why we decide to exploit the invariant $J(S)$, and the related equation in (16), for the computation of the shape fitting cylinders. More precisely, we start from

$$\pi\cdot h^3 - 12\cdot\pi\cdot J(S)\cdot h+6 = 0 \tag{17}$$

and compute the parameters h, that uniquely (up to isometric transformations) define the corresponding unit volume cylinder $C\left(h, a=\frac{1}{\sqrt{\pi\cdot h}}\right)$. It turns out that, with small exceptions, there are two parameters h, satisfying the conditions above.

The equation in (17) is a cubic equation in h. The number of solutions (roots) of (17) depends on the, so called, discriminant Δ, as follows:

- if $\Delta > 0$, the equation in (17) has three real solutions;
- if $\Delta = 0$, the equation in (17) has one multiple real solution;
- if $\Delta < 0$, the equation in (17) has one real solution and two complex ones.

In the case observed here, the discriminant Δ is as follows

$$\Delta \;=\; 108 \cdot \pi^2 \cdot \left(64 \cdot \pi^2 \cdot J(S)^3 - 9\right). \tag{18}$$

Of course, we are interested in the positive values of h, that are solutions of the equation in (17). This is because h has a clear geometric interpretation – the cylinder height (see Fig.1).

The quantity $J(S)$ is not bounded above (i.e. $J(S)$ can be arbitrarily large) but reaches its minimal possible value if S is a $3D$ ball (i.e. a shape bounded by a perfect $3D$ sphere) [35, 36]. The following estimate gives the best possible lower bound [35, 36]:

$$J(S) \;\geq\; \frac{3^{5/3}}{5 \cdot (4\pi)^{2/3}} \;\approx\; 0.2309, \tag{19}$$

with the equality, in (19), if and only if S is a $3D$ ball [35, 36].

Thus, an immediate observation would say, the discriminant Δ (for an arbitrary shape S) defined as in (18), is inside the interval

$$\begin{aligned} & \left[108 \cdot \pi^2 \cdot \left(64 \cdot \pi^2 \cdot \left(\frac{3^{5/3}}{5 \cdot (4\pi)^{2/3}}\right)^3 - 9\right),\ \infty\right) \\ & \left[108 \cdot \pi^2 \cdot \left(\frac{4 \cdot 3^5}{125} - 9\right),\ \infty\right) \\ \approx\ & [-1304.7,\ \ \infty). \end{aligned} \tag{20}$$

So, observing the range of $J(S)$ only, all three situations $\Delta > 0$, $\Delta = 0$, and $\Delta < 0$, would be possible.

Note 1 *The lower bound for $J(S)$, if S is a perfect cylinder is, of course, larger than the lower bound in (19). If we start from the second equality in (15), we have*

$$\frac{dJ(C(h,a))}{dh} \;=\; \frac{-1}{2 \cdot \pi \cdot h^2} + \frac{h}{6}. \tag{21}$$

So, the equation $\dfrac{dJ(C(h,a))}{dh} = 0$ *has a single solution:* $h = \sqrt[3]{\dfrac{3}{\pi}}$. *Further, since*

$$\lim_{h \to 0} J(C(h,a)) = \lim_{h \to \infty} J(C(h,a)) = \infty,$$

we deduce (taking into account the scaling invariance of $J(S)$) that the minimum value of the $J(S)$, if S is a perfect cylinder, is reached for $h = \sqrt[3]{\frac{3}{\pi}}$ *and is calculated as follows*

$$\begin{aligned} & \min\{J(C(h,a)) \mid C(h,a) \text{ is a cylinder}\} \\ = \;& J\left(C\left(h = \sqrt[3]{\frac{3}{\pi}}\right),\ a = \frac{1}{\sqrt[6]{3\cdot\pi^2}},\right) \\ = \;& J(C(h \approx 0.9847, a \approx 0.5685)) \\ = \;& \frac{3}{4\cdot\sqrt[3]{3\cdot\pi^2}} \;\approx\; 0.2424. \end{aligned} \tag{22}$$

Note 2 *There is a short interval*

$$I = \left[\frac{3^{5/3}}{5\cdot(4\pi)^{2/3}},\ \frac{3}{4\cdot\sqrt[3]{3\cdot\pi^2}}\right) \;\approx\; [0.2309,\ 0.2424) \tag{23}$$

such that $J(C(h)) \notin I$, *for all* h*. The shapes* S *whose* $J(S)$ *values are inside* I *are nearly spherical and all of them are best matched (in terms considered here) by the cylinder* $J\left(C\left(\frac{1}{\sqrt[6]{3\cdot\pi^2}},\ \sqrt[3]{\frac{3}{\pi}}\right)\right)$, *as described in (22). This is not of a great importance for us now, since this work is aimed to analyze more 'elongated' 3D shapes. For such, 'not nearly spherical', shapes* $J(S)$ *is larger than* $\frac{3}{4\cdot\sqrt[3]{3\cdot\pi^2}} \approx 0.2424$.

So far, we have shown that there are just a finite number (up to three) candidates for the cylinders that fit well with the shape considered. Next, we show even more, that the method does offer exactly two fitting cylinders, for any shape S with $J(S) \notin I$ (see (23)). We show this in two steps (the next two items).

- In the case of $\Delta < 0$, not all the three solutions of the equation in (17) can be positive. Indeed, if h_1, h_2, and h_3, are roots of the equation in (17) then

$$\begin{aligned} & \pi\cdot h^3 - 12\cdot\pi\cdot J(S)\cdot h + 6 \\ = \;& \pi\cdot(h-h_1)\cdot(h-h_2)\cdot(h-h_3), \end{aligned} \tag{24}$$

  and further

$$\begin{aligned} & -h_1 - h_2 - h_3 = 0, \\ & h_1\cdot h_2 + h_1\cdot h_3 + h_2\cdot h_3 = -12\cdot J(S), \\ & -\pi\cdot h_1\cdot h_2\cdot h_3 = 6. \end{aligned} \tag{25}$$

  However, if $h_1 \geq 0$, $h_2 \geq 0$, and $h_3 \geq 0$ is assumed, then $h_1\cdot h_2 + h_1\cdot h_3 + h_2\cdot h_3 > 0$. Consequently, the second equality $h_1\cdot h_2 + h_1\cdot h_3 + h_2\cdot h_3 = -12\cdot J(S)$, in (25), would contradict to the fact that $J(S) > 0$, for any shape S.

- Similarly to the above, we deduce a contradiction if we assume only one root, let say h_1, in (17) to be positive. Then, it must be $h_2 \cdot h_3 > 0$. This further would contradict to $-\pi \cdot h_1 \cdot h_2 \cdot h_3 = 6$, (from (25)), since the left part of the last equality would be a negative number, i.e. cannot be equal to 6.

Thus, exactly two zeros of the equality in (17) are positive. More details are in the following note.

Note 3 *If two zeros, let say h_1 and h_2, in the polynomial in (24) are equal then $h_1 = h_2 = \sqrt[3]{\frac{3}{\pi}}$. In such a case, the third zero h_3 is negative and satisfies $h_3 = -2 \cdot \sqrt[3]{\frac{3}{\pi}}$. In other words, this is the only case where the fitting cylinders coincide. Such a fitting cylinder is $C\left(h = \sqrt[3]{\frac{3}{\pi}},\ a = \frac{1}{\sqrt[6]{3 \cdot \pi^2}}\right)$, i.e. the cylinder that has the minimal possible value of the $3D$ invariant $J(S)$ (see Note 1 and derivation of the equality in (22)).*

Now, since we know that the number of solutions of the equation in (17) is exactly two, we give the following definition of the cylinders fitting with a given $3D$ shape.

Definition 1 *Let a $3D$ shape, with $J(S) \notin I$, be given. Then we define two fitting cylinders*

$$C(h_l) = C\left(h_l, a_s = \frac{1}{\sqrt{\pi \cdot h_l}}\right) \tag{26}$$

$$C(h_s) = C\left(h_s, a_l = \frac{1}{\sqrt{\pi \cdot h_s}}\right) \tag{27}$$

for the shape S. The parameters h_l and h_s are solutions of the following equation (see (17)) [2]*:*

$$\pi \cdot h^3 - 12 \cdot \pi \cdot J(S) \cdot h + 6 \; = \; 0.$$

We assume $h_l > h_s$ (i.e. indicies l and s stand for 'long' and 'short', respectively).

3.1 Fitting Cylinders Examples

We proceed with several examples that include shapes selected randomly and their corresponded fitting cylinders, computed based on the equation in (17). These examples are in Fig.2. Four $3D$ shapes are selected randomly from the well known *McGill 3D Shape Benchmark* shape data set [20]. They are displayed in the first row in Fig.2, and their names, as given in the data set [20], are immediately below them. Their corresponding fitting cylinders are displayed below them[3],

[2]This is a cubic equation, whose solutions can be given in an explicit (but slightly complicated) form, by using Cardano's result.

[3]Notice that the fitting cylinders, in Fig.2, are presented by their oval surfaces only – not as $3D$ closed bodies, as they are. This has been done for a better visualization purpose.

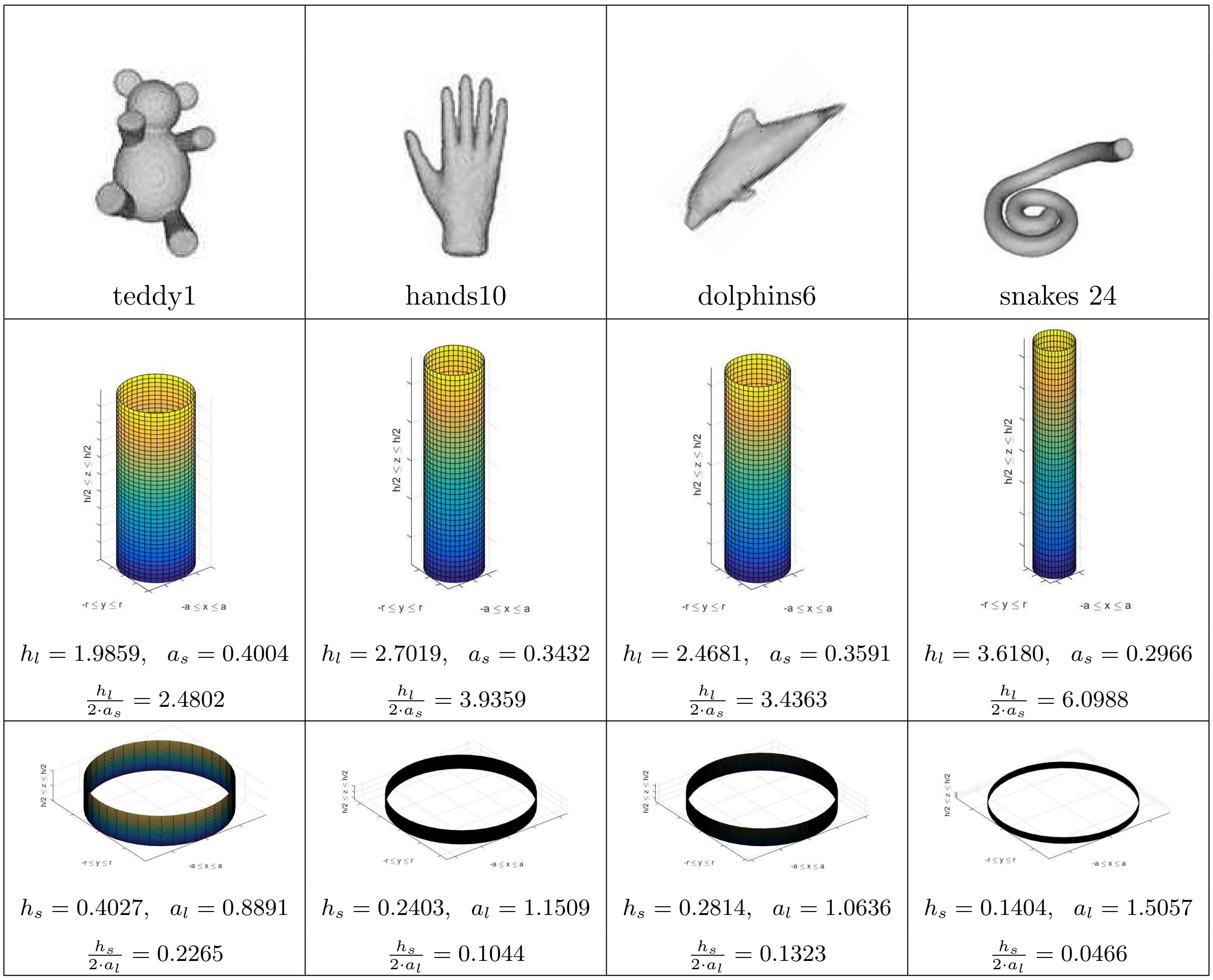

Figure 2: Four shapes, selected randomly, from [20] data set are in the first row. Their fitting cylinders are given below them, together with the positive zeros h_l and h_s, computed from the related equality in (17). The parameters $a_s = 1/\sqrt{\pi \cdot h_l}$, $a_l = 1/\sqrt{\pi \cdot h_s}$, $h_l/(2 \cdot a_s)$, and $h_s/(2 \cdot a_l)$, are also given, for better illustration purposes.

together with the corresponding h_l and h_s values necessary for their computation. The larger, positive zero h_l of the equation in (17) determines a more 'elongated' fitting cylinder, while the smaller positive zero of the equation in (17) determines the cylinder that is less elongated. The values $a_s = \dfrac{1}{\sqrt{\pi \cdot h_l}}$ and $a_l = \dfrac{1}{\sqrt{\pi \cdot h_s}}$, that correspond to the values h_l and h_s, respectively, are also given. The corresponding values $\dfrac{h_l}{2 \cdot a_s}$ and $\dfrac{h_s}{2 \cdot a_l}$ are also provided, in order to illustrate how much the fitting cylinders are elongated.

At the moment, it seems reasonable to say that the first, second and third shape, in the first row, are better fitted with the more elongated cylinder (determined by the bigger h value (i.e. by the computed parameter h_l). The fourth shape (in the first row) does look to be far away from a cylindrical shapes. This is why is difficult to have a perception which of two computed fit cylinders would be a better fit to the shape displayed. A method to evaluate numerically how good is fitting between the shape considered and their related fitting cylinders, as well as properties of such the method, will be discussed in the following section.

More shapes and their corresponding fitting cylinders can be found in the Fig.3-6. This time the fitting cylinders are given by their unique parameters h_l and h_s, but they are not displayed, as it has been done in Fig.2.

4 Cylinderness Measure for $3D$ Shapes

In this section we observe how a comparison between the shape given and its two fitting cylinders, could lead a numerical evaluation of how much a shape given looks like a cylinder[4] Such a computed quantity will be called the *shape cylinderness measure.*

As it has been shown, there are two solutions h_l and h_s of the equation in (17), and these solutions define two fitting cylinders

$$C\left(h_l, a_s = \frac{1}{\sqrt{\pi \cdot h_l}}\right) \quad \text{and} \quad C\left(h_s, a_l = \frac{1}{\sqrt{\pi \cdot h_s}}\right). \tag{28}$$

There are many ways how two shapes can be compared. Herein we will employ a very general one, that can applied to arbitrary pair of shapes. Such a shape comparison leads to two quantities, $\mathcal{C}_a(S)$ and $\mathcal{C}_b(S)$ (see Definition 2), and further to the new $3D$ shape cylinderness measure, as given in Definition 3.

Later on, in the next section, we will describe a modified measure that simplifies the computation, still keeps nice measure properties, but slightly reduces the situations were it can be applied directly (to the highly symmetric shapes, for example).

[4]Notice that a comparison with just one of these fitting cylinders does not lead to the measure satisfying the desirable properties like those listed in the Theorem1. This is, for example, because $\mathcal{C}_a(S) = \mathcal{C}_b(S) = 1$ cannot be true for an arbitrary shape (cylinder) S. More precisely, $\mathcal{C}_a(S) = \mathcal{C}_b(S) = 1$ would imply that S coincides with both fitting cylinders corresponding to the parameters a and b. This is not possible.

Definition 2 *Let a $3D$ shape S be given. Let the volume of S be equal to 1 and the centroid of S be coincident with the origin. We define two auxiliary quantities $\mathcal{C}_a(S)$ and $\mathcal{C}_b(S)$ as follows:*

$$\mathcal{C}_a(S) \;=\; \max_{S(\alpha)} \left\{ \frac{Volume\left(S(\alpha)\ \cap\ C\left(h_l, a_s\right)\right)}{Volume\left(C\left(h_l, a_s\right)\right)} \right\} \tag{29}$$

$$\mathcal{C}_b(S) \;=\; \max_{S(\alpha)} \left\{ \frac{Volume\left(S(\alpha)\ \cap\ C\left(h_s, a_l\right)\right)}{Volume\left(C\left(h_s, a_l\right)\right)} \right\} \tag{30}$$

where

– h_l and h_s are zeros of the equation in (17), allocated to the shape S;

– $a_s = \frac{1}{\sqrt{\pi \cdot h_l}}$, $a_l = \frac{1}{\sqrt{\pi \cdot h_s}}$;

– $C(h_l, a_s)$ and $C(h_s, a_l)$ are cylinders defined as in (6); and finally,

– $S(\alpha)$ is a shape obtained by an arbitrary rotation of the shape S around its centroid.

Now, we are able to give a formal definition of the new cylinderness measure, denoted by $\mathbf{C}(S)$.

Definition 3 *Let a shape S, whose volume is equal to 1 and whose centroid coincides with the origin, be given. The $3D$ shape cylinderness measure, $\mathbf{C}(S)$, is defined as follows:*

$$\mathbf{C}(S) \;=\; \max\left\{\mathcal{C}_a(S),\ \mathcal{C}_b(S)\right\} \tag{31}$$

where $\mathcal{C}_a(S)$ and $\mathcal{C}_b(S)$ are as in (29) and (30), respectively.

The next theorem lists important properties of the measure $\mathcal{C}(S)$.

Theorem 1 *The cylinderness measure $\mathbf{C}(S)$ has the following properties:*

(a) $\mathbf{C}(S) \in [0,1]$, *for all the $3D$ shapes S;*

(b) $\mathbf{C}(S) = 1 \quad \Leftrightarrow \quad S$ *is a cylinder;*

(c) $\mathbf{C}(S)$ *is invariant with respect to the translations, rotations, and scaling transformations.*

Proof. The items (a) and (c) follow from the definition. To prove (b) let us assume that S_0 is a unit volume cylinder $C\left(h_0, a_0\right)$, defined by the parameters $h = h_0$ and $a_0 = \frac{1}{\sqrt{\pi \cdot h_0}}$, as given in (6). This further means

$$J(S_0) \;=\; \frac{1}{2 \cdot \pi \cdot h_0} + \frac{h_0^2}{12} \tag{32}$$

based on (15). Entering the equality in (32) into (17), we get

$$\pi \cdot h^3 - 12 \cdot \pi \cdot h \cdot \left(\frac{1}{2 \cdot \pi \cdot h_0} + \frac{h_0^2}{12} \right) + 6 \;=\; 0. \tag{33}$$

The equality in (33) is equivalent to

$$\pi \cdot (h - h_0) \cdot \left(h \cdot (h + h_0) - \frac{6}{\pi \cdot h_0} \right) \; = \; 0. \tag{34}$$

Thus, $h = h_0$ is the solution of the equation in (33), and the method offers the cylinder $C\left(h_0, a = \frac{1}{\sqrt{\pi \cdot h_0}}\right)$, as one of the best fitted cylinders to the given shape S_0. Since $S_0 = C\left(h_0, a = \frac{1}{\sqrt{\pi \cdot h_0}}\right)$, this further means that either $\mathcal{C}_1(S_0) = 1$ or $\mathcal{C}_2(S_0) = 1$, is true (see (29) and (30)). So, $\mathbf{C}(S_0) = 1$ is proven, due to the equality/definition in (37).

On the other side, if $\mathbf{C}(S_0) = 1$ then it must be either $\mathcal{C}_a(S_0) = 1$ or $\mathcal{C}_b(S_0) = 1$. Due to the definitions in (29) and (30), the shape S_0 must coincide with one of the fitting cylinders, $C(h_l, a_s)$ and $C(h_s, a_l)$, where h_l and h_s are the solutions of the equation in (17). This establishes the proof. □

5 Experimental Section

In this section, first, we give a modified version of the cylinderness measure established in the previous section. Then, we provide several experiments in order to enable a better understanding how the modified cylinderness measure behaves. All experiments also include the unique parameters (h_l and h_s), necessary to reconstruct the fitting cylinders, related to the shapes considered. This time the cylinders are not displayed, as this has been done in Fig. 2

5.1 A Modified Cylinderness Measure

Till now, all the theoretical framework was established by working in a continuous space. However, in image processing and computer vision tasks, and more generally, in images technology based object analysis procedures, we deal with computer images - i.e. in situations where real $3D$ objects are presented with the sets of voxels inside the objects. Because of that, the maxima in (29) and (30) can be only computed numerically. Of course, this always causes an inherent error. Such an error is not large, in this particular case. This is because the volumes of $3D$ regions, as required in (29) and (30), can be approximated efficiently just by enumerating the integer points (voxels) inside the $3D$ region considered [4, 11].

A straightforward numerical computation of the maximums in (29) and (30), by using incremental angles rotations around the object centroid, can be time consuming, particularly if the objects considered are represented by a high $3D$ image resolution, i.e. if the objects consist of a large number of voxels.

Because of the above, we will relax conditions in Definition 2, in order to preserve a simpler computation. We propose efficient substitutes for the quantities $\mathcal{C}_a(S)$ and $\mathcal{C}_b(S)$, and the cylinderness measure $\mathbf{C}(S)$, (see Definition 3), that can be computed without a use of any incremental optimizing procedure. More precisely, the shapes considered are oriented such that their principal axes [5] coincide with the principal axes of their fitting cylinders, and all the necessary computations are done without any additional incremental rotations of the shapes measured. All the theoretical observations and the statements made are analogue to those in the previous sections. The key statements still remain valid for the modified measure, as in the case of the $\mathbf{C}(S)$ measure. Thus, the proofs are omitted.

Definition 4 *Let a* $3D$ *shape* S *be given. Let the volume of* S *be equal to* 1 *and the centroid of* S *be coincident with the origin. We define two following quantities* $\mathcal{C}_1(S)$ *and* $\mathcal{C}_2(S)$ *as follows:*

$$\mathcal{C}_1(S) \;=\; \max_{S(\beta)} \left\{ \frac{Volume\,(S(\beta)\ \cap\ C\,(h_l, a_s))}{Volume\,(C\,(h_l, a_s))} \right\} \tag{35}$$

$$\mathcal{C}_2(S) \;=\; \max_{S(\beta)} \left\{ \frac{Volume\,(S(\beta)\ \cap\ C\,(h_s, a_l))}{Volume\,(C\,(h_s, a_l))} \right\} \tag{36}$$

where $S(\beta)$ *equals the shape* S *oriented such that its principal axes coincide with the principal axes of the fitting cylinders* $C\,(h_l, a_s)$ *and* $C\,(h_s, a_l)$[5].

Now, we are able to give a formal definition of the measure $\mathcal{C}(S)$ that is a modification of the $\mathbf{C}(S)$ measure.

Definition 5 *Let a shape* S*, whose volume is equal to* 1 *and whose centroid coincides with the origin, be given. The* $3D$ *shape cylinderness measure,* $\mathcal{C}(S)$*, is defined as follows:*

$$\mathcal{C}(S) \;=\; \max\left\{\mathcal{C}_1(S),\ \mathcal{C}_2(S)\right\} \tag{37}$$

where $\mathcal{C}_1(S)$ *and* $\mathcal{C}_2(S)$ *are as in (35) and (36), respectively.*

Note 4 *The time complexity of the initial method for the computation of the cylinderness measure varies depending on the number of incremental rotations required (see Definition 2). It goes from*
– an asymptotically optimal time complexity of $\mathcal{O}(N)$ *(*N *is the number of shape points) if the number of incremental rotations is fixed;*
to
– an unbounded complexity, if the number of incremental rotation used, is unbounded too.

Thus, the dominance of the modified method, compared to the one based on Definition 2, can be significant if the number of incremental rotations used is big enough.

The next theorem lists desirable properties of the measure $\mathcal{C}(S)$. These properties are analogue to the properties of the $\mathbf{C}(S)$ measure (see Theorem 1).

[5] We still use the maximum operator in (35) and (36), but there are no more than 8 choices for β. Just to mention that the number of α values in (29) and (30) can be selected to be arbitrary large.

Theorem 2 *The cylinderness measure $\mathcal{C}(S)$ has the following properties:*

(a) $\mathcal{C}(S) \in [0,1]$, *for all the* $3D$ *shapes* S;

(b) $\mathcal{C}(S) = 1 \quad \Leftrightarrow \quad S$ *is a cylinder*;

(c) $\mathcal{C}(S)$ *is invariant with respect to the translations, rotations, and scaling transformations.*

We start our experiments with synthetics shapes. After that we use a relatively small collection of shapes from the well know data set [20]. The results obtained are reasonable, and we may say, fit well with human perception.

As it has been mentioned, in all the experiments we had to work on discretized data – i.e. on the objects presented by the sets of voxels. This is why all computed values and parameters are approximate ones, and given as decimal numbers.

5.2 Experiments on Synthetic Data

To illustrate the behavior of the new measure $\mathcal{C}(S)$ we have used a $3D$ cube stretched/shrunk for different coefficients, in direction of the coordinate axes. The results are given in Fig.3. Five objects are considered. The first object, in the first row, is a regular cube. It has relatively high cylinderness measure ($\mathcal{C}(S) = 0.8458$). It is worth noticing that the corresponding values $\mathcal{C}_1(S) = 0.8458$ and $\mathcal{C}_2(S) = 0.7875$ are relatively close. This can be explained by a relatively high N-fold symmetry of a regular cube. The next two shapes, whose edge-length ratio differs essentially (i.e. these are $1 \times 1 \times 2$ and $1 \times 1 \times 8$) have almost the same computed cylinderness measure, 0.9093 and 0.9091, respectively This is not a surprise taking into account that both measured $3D$ shapes have a square as the base, instead of the circle. This is the only difference from a perfect cylinder.

Anyhow, once the shape S varies, its allocated fitting cylinders vary, as well (even though the corresponded cylinderness measure may stay the same). Indeed, for the second and third shape, in Fig.3 these cylinders are determined by the parameters, that differs very much, $h_l = 1.5846$ and $h_s = 0.5616$ (for the second shape), and $h_l = 3.8909$ and $h_s = 0.1223$ (for the third shape). However, the comparison of the second shape with allocated fitting cylinder $C(h_l = 1.5846)$ and comparison of the third shape with the allocated fitting cylinder $C(h_l = 3.8909)$ leads to almost identical cylinderness measures (0.9093 and 0.9091 respectively). It might be worth noticing that their comparison with the corresponding fitting cylinders $C(h_s = 0.5626)$ and $C(h_s = 0.1223)$ leads to the essentially different scores of $\mathcal{C}_2(S) = 0.6562$ and $\mathcal{C}_2(S) = 0.1967$, respectively.

Regarding the fourth and fifth shape in the first row in Fig.3, we notice that the computed cylinderness measures are obtained by comparing these shapes with the cylinders $C(h_s = 0.3871)$ and $C(h_s = 0.2466)$. In other words, the method says that these shapes are more similar to the less

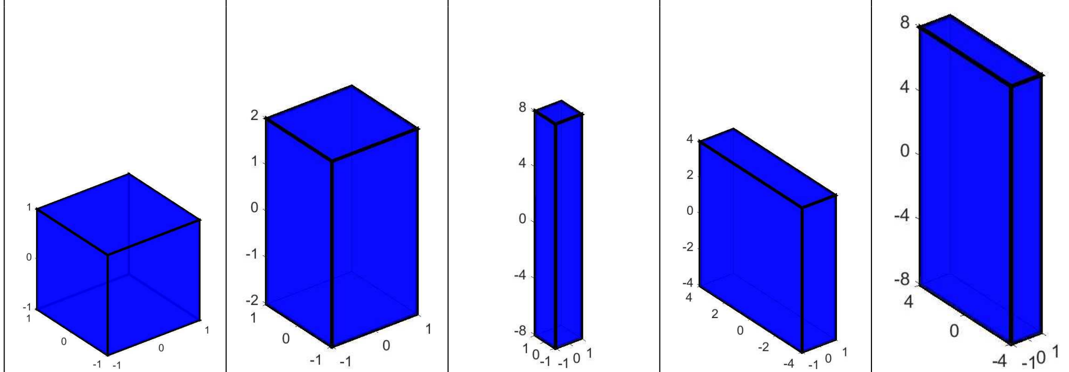

$1 \times 1 \times 1$	$1 \times 1 \times 2$	$1 \times 1 \times 8$	$1 \times 4 \times 4$	$1 \times 4 \times 8$
$h_l = 1.1613$	$h_l = 1.5846$	$h_l = 3.8909$	$h_l = 2.0359$	$h_l = 2.6625$
$\frac{h_l}{2 \cdot a_s} = 1.1091$	$\frac{h_l}{2 \cdot a_s} = 1.7678$	$\frac{h_l}{2 \cdot a_s} = 6.8017$	$\frac{h_l}{2 \cdot a_s} = 2.5744$	$\frac{h_l}{2 \cdot a_s} = 3.8502$
$\mathcal{C}_1(S) = 0.8458$	$\mathcal{C}_1(S) = 0.9093$	$\mathcal{C}_1(S) = 0.9091$	$\mathcal{C}_1(S) = 0.4826$	$\mathcal{C}_1(S) = 0.5344$
$h_s = 0.8271$	$h_s = 0.5616$	$h_s = 0.1223$	$h_s = 0.3871$	$h_s = 0.2466$
$\frac{h_s}{2 \cdot a_l} = 0.6666$	$\frac{h_s}{2 \cdot a_l} = 0.3730$	$\frac{h_s}{2 \cdot a_l} = 0.0379$	$\frac{h_s}{2 \cdot a_l} = 0.2134$	$\frac{h_s}{2 \cdot a_l} = 0.1085$
$\mathcal{C}_2(S) = 0.7875$	$\mathcal{C}_2(S) = 0.6562$	$\mathcal{C}_2(S) = 0.1967$	$\mathcal{C}_2(S) = 0.8391$	$\mathcal{C}_2(S) = 0.7024$
$\mathcal{C}(S) = 0.8458$	$\mathcal{C}(S) = 0.9093$	$\mathcal{C}(S) = 0.9091$	$\mathcal{C}(S) = 0.8391$	$\mathcal{C}(S) = 0.7024$

Figure 3: Five shapes obtained by stretching a cube, for different coefficients, are in the first row. The edge-length ratios are immediately below the shapes obtained. The parameters of the corresponding fitting cylinders are also given, as well as the computed quantities $\mathcal{C}_1(S)$ and $\mathcal{C}_2(S)$, for each of the shapes considered. The computed cylinderness measure values are in the last row.

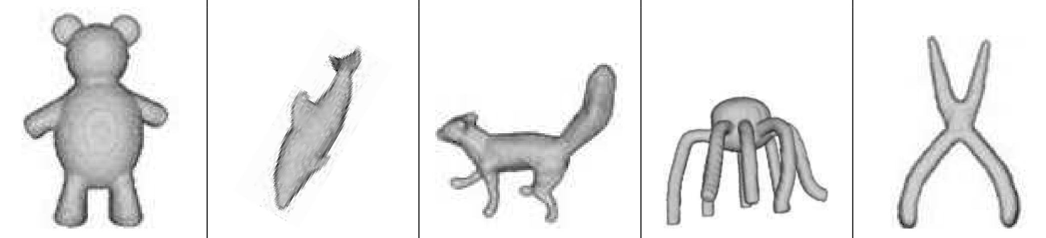

teddy10	dolphins3	four29	octopuses4	pliers2
$h_l = 2.0936$	$h_l = 2.5487$	$h_l = 3.0153$	$h_l = 2.9769$	$h_l = 4.1306$
$\frac{h_l}{2 \cdot a_s} = 2.6846$	$\frac{h_l}{2 \cdot a_s} = 3.6060$	$\frac{h_l}{2 \cdot a_s} = 4.6402$	$\frac{h_l}{2 \cdot a_s} = 4.5519$	$\frac{h_l}{2 \cdot a_s} = 7.43994$
$\mathcal{C}_1(S) = 0.7447$	$\mathcal{C}_1(S) = 0.7770$	$\mathcal{C}_1(S) = 0.5447$	$\mathcal{C}_1(S) = 0.2689$	$\mathcal{C}_1(S) = 0.2034$
$h_s = 0.3702$	$h_s = 0.2848$	$h_s = 0.1972$	$h_s = 0.2018$	$h_s = 0.1091$
$\frac{h_s}{2 \cdot a_l} = 0.1996$	$\frac{h_s}{2 \cdot a_l} = 0.1217$	$\frac{h_s}{2 \cdot a_l} = 0.0776$	$\frac{h_s}{2 \cdot a_l} = 0.0803$	$\frac{h_s}{2 \cdot a_l} = 0.0319$
$\mathcal{C}_2(S) = 0.5669$	$\mathcal{C}_2(S) = 0.4343$	$\mathcal{C}_2(S) = 0.3029$	$\mathcal{C}_2(S) = 0.1595$	$\mathcal{C}_2(S) = 0.2326$
$\mathcal{C}(S) = 0.7447$	$\mathcal{C}(S) = 0.7770$	$\mathcal{C}(S) = 0.5447$	$\mathcal{C}(S) = 0.2689$	$\mathcal{C}(S) = 0.2326$

Figure 4: Five shapes from different classes in [20] are in the first row. The related parameters (h_l, $h_l/(2 \cdot a_s)$, $\mathcal{C}_1(S)$, h_s, $h_s/(2 \cdot a_l)$, and $\mathcal{C}_2(S)$) are displayed below the corresponding shapes. The cylinderness measures $\mathcal{C}(S)$ computed are in the last row.

elongated cylinders (in the sense of the $h_s/(2 \cdot a_s)$ and $h_s/(2 \cdot a_l)$ ratios) than to the (more elongated) cylinders determined by larger h_l values (i.e. the cylinders $C(h_l = 2.0359)$ and $C(h_l = 2.6625)$).

This might be understood as expected and intuitively clear outcome and confirmation that both fitting cylinders have to be taken into account if we would like to compute the cylinderness measure of of the shapes considered.

5.3 Experiments on a Known $3D$ Shapes Data-set Examples

In this subsections we have used shapes from the well-known data-set [20].

– Five shapes, in Fig.4, are selected randomly from different shape classes, and their cylinderness measures are computed. The related parameters h_l and h_s, of the corresponding fitting cylinders, the visualizations supporting ratios $h_l/(2 \cdot a_s)$ and $h_s/(2 \cdot a_l)$, and related quantities $\mathcal{C}_1(S)$ and $\mathcal{C}_2(S)$ are also provided.

The obtained results might be understood as expected ones. The highest cylinderness measure is computed for the first two shapes. The third shape is 'bended' slightly, which has caused a

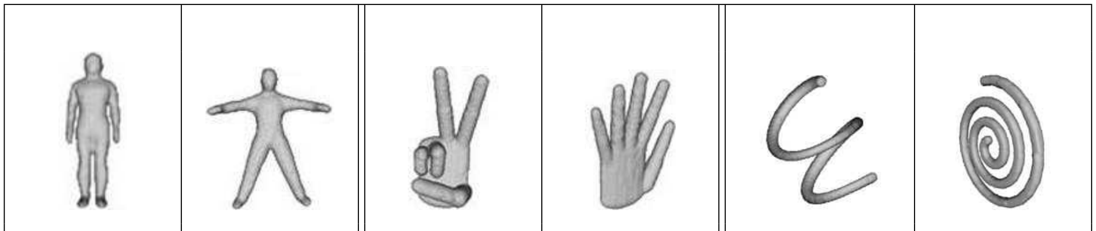

humans15	humans17	hands3	hands2	snakes14	snakes25
$h_l = 3.1464$	$h_l = 3.6370$	$h_l = 3.4002$	$h_l = 3.0174$	$h_l = 5.2855$	$h_l = 4.7292$
$\frac{h_l}{2 \cdot a_s} = 4.9461$	$\frac{h_l}{2 \cdot a_s} = 6.1470$	$\frac{h_l}{2 \cdot a_s} = 5.5565$	$\frac{h_l}{2 \cdot a_s} = 4.6451$	$\frac{h_l}{2 \cdot a_s} = 10.7690$	$\frac{h_l}{2 \cdot a_s} = 9.1144$
$\mathcal{C}_1 = 0.6723$	$\mathcal{C}_1 = 0.4794$	$\mathcal{C}_1 = 0.6396$	$\mathcal{C}_1 = 0.6606$	$\mathcal{C}_1 = 0.0667$	$\mathcal{C}_1 = 0.3260$
$h_s = 0.1824$	$h_s = 0.1391$	$h_s = 0.1579$	$h_s = 0.1969$	$h_s = 0.0675$	$h_s = 0.0839$
$\frac{h_s}{2 \cdot a_l} = 0.0690$	$\frac{h_s}{2 \cdot a_l} = 0.0460$	$\frac{h_s}{2 \cdot a_l} = 0.0556$	$\frac{h_s}{2 \cdot a_l} = 0.0774$	$\frac{h_s}{2 \cdot a_l} = 0.0155$	$\frac{h_s}{2 \cdot a_l} = 0.0215$
$\mathcal{C}_2 = 0.3853$	$\mathcal{C}_2 = 0.3025$	$\mathcal{C}_2 = 0.3427$	$\mathcal{C}_2 = 0.3977$	$\mathcal{C}_2 = 0.0478$	$\mathcal{C}_2 = 0.4122$
$\mathcal{C} = 0.6723$	$\mathcal{C} = 0.4794$	$\mathcal{C} = 0.6396$	$\mathcal{C} = 0.6606$	$\mathcal{C} = 0.0667$	$\mathcal{C} = 0.4122$

Figure 5: Three pairs of shapes, from the data set [20], are used to illustrate the $\mathcal{C}(S)$ behavior under the shape deformation transformations. Immediately below the shapes are their names as given in [20]. The related shape parameters and the quantities $\mathcal{C}_1(S)$ and $\mathcal{C}_2(S)$ are also provided. The measured shape cylinderness values are in the last row.

decrease in the cylinderness measure computed. The lowest cylinderness measure is computed for the pliers shape (the shape on the right). This is also in accordance with our perception. It might be worth mentioning that the cylinderness measure for this pliers shape comes from the shape comparison with the cylinder determined by the smaller computed h (i.e. h_s) value. The rest of the shapes, in Fig.4 fit better with the cylinder determined by the higher h (i.e. h_l) value, computed from the equation in (17).

– The behavior of the new cylinderness measure $\mathcal{C}(S)$ under the shape deformation transformations is illustrated by examples in Fig.5. Three pairs of shapes, from different classes in [20], are considered. The second shape in each pair of shapes presented can be understood as the first shape (in the related pair) subjected to certain level of a deformation transform. Depending on the level of deformation applied, the computed $\mathcal{C}(S)$ values vary differently. The largest difference is computed for two 'snake' shapes (the last two shapes in the first row). The same could be said for the related quantities $\mathcal{C}_1(S)$ and $\mathcal{C}_2(S)$ inside of each pair.

5.4 Robustness under Erosion Transformation

In the next experiments we consider the robustness of the new measure, under erosion transformations. We have used a cylinder whose height is $h = 20.02$ the base radius is $a = 4.2$. As it has been mentioned, herein we have to work with the discretized real objects. So, the cylinder observed is represented by using the cubes/voxels of the size $1 \times 1 \times 1$. In this particular case, the number of voxels, whose centers belong to the cylinder observed, was 1092. The discretized/voxelized cylinder is displayed on the left, in Fig.6. The voxel centers, in the shapes in Fig.6, are represented by the dots. For such obtained voxelized data, the shape of the original cylinder shape is estimated to be equal to the shape of a unit volume cylinder $C(h = 2.0361)$ (i.e. with the parameter $h_l = 2.0361$). It has turned out, the estimated cylinderness measure was equal to 1. In other words, it has happened that all the scaled voxels, belonging to the normalized observed cylinder, were inside the fitting cylinder $C(h_l = 2.0361)$, as well. It is worth mentioning that for another choice of digitized cylinder (whose parameters differ from $h = 20.02$ and $a = 4.2$.), the estimated cylinderness may vary.

Next, we have removed a certain number of voxels from the original cylinder (i.e. its discretization). These voxels are selected randomly. For the second, third, and fourth shape, in the first row in Fig.6, the number of voxels removed were nearly 10%, 20%, and 40%, respectively. The exact number of voxels, remaining to represent the initial shape, is given immediately below the shapes related. Roughly speaking, the computed cylinderness measure $\mathcal{C}(S)$, of such eroded shape, has been changed (decreased) accordingly to the percentage of the voxels removed. It is up to the readers to judge is the presented robustness good enough for their possible applications.

We also have provided the data (i.e. h_l and h_s values) showing how do fitting cylinders (allocated the shapes eroded) changes under such erosion transformations applied. Again, we leave the judgment of the quality of the results obtained to the readers. Surely, the judgment would depend on the application planned to be done.

Comments similar to the comments above apply to the first shape in the second row, even though the erosion level is very high (more than 50% voxels were removed). The last two shapes, in the second row, are given to illustrate that the cylinderness measure $\mathcal{C}(S)$ can be applied to an arbitrary set of $3D$ points (or voxels), not necessary to the point-sets that do suggest that they represent connected $3D$ objects, or $3D$ objects of a specific class (in this case the digitized $3D$ cylinders). Thus, very small $\mathcal{C}(S)$ values, for the last two shapes, are not surprising.

6 Concluding Remarks

A theoretical framework has been established to solve a cylinder fitting problem for $3D$ shapes. It has been turned out that the method established allocates two fitting cylinders for any of $3D$ shapes,

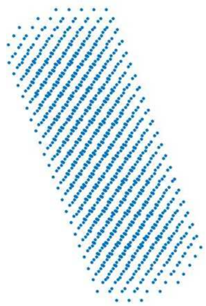 1092 voxels	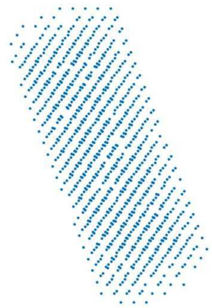 1000 voxels	 900 voxels	 700 voxels
$h_l = 2.0361$ $\mathcal{C}_1 = 1$	$h_l = 2.1096$ $\mathcal{C}_1 = 0.9260$	$h_l = 2.2153$ $\mathcal{C}_1 = 0.7922$	$h_l = 2.4396$ $\mathcal{C}_1 = 0.6257$
$h_s = 0.3871$ $\mathcal{C}_2 = 0.5522$	$h_s = 0.3657$ $\mathcal{C}_2 = 0.5050$	$h_s = 0.3377$ $\mathcal{C}_2 = 0.3029$	$h_s = 0.2871$ $\mathcal{C}_2 = 0.3629$
$\mathcal{C}(S) = 1$	$\mathcal{C}(S) = 0.9260$	$\mathcal{C}(S) = 0.7922$	$\mathcal{C}(S) = 0.62579$

	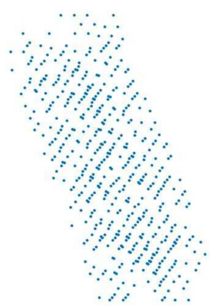 500 voxels	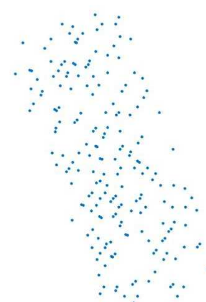 300 voxels	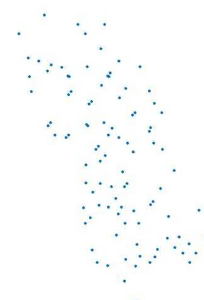 100 voxels
	$h_l = 2.7632$ $\mathcal{C}_1 = 0.4540$	$h_l = 3.9895$ $\mathcal{C}_1 = 0.1900$	$h_l = 4.7270$ $\mathcal{C}_1 = 0.0700$
	$h_s = 0.2308$ $\mathcal{C}_2 = 0.2840$	$h_s = 0.1166$ $\mathcal{C}_2 = 0.1050$	$h_s = 0.0840$ $\mathcal{C}_2 = 0.0500$
	$\mathcal{C}(S) = 0.4540$	$\mathcal{C}(S) = 0.1602$	$\mathcal{C}(S) = 0.0700$

Figure 6: The discrete point set in the first row on the left represents a cylinder discretized on a regular $3D$ integer grid. The rest of the shapes are obtained by removing a certain number of points from the shape on the left. The number of the points removed is immediately below the shapes. The rest of voxels were used to approximate cylinderness measure $\mathcal{C}$ of such discrete point sets, consisting of unit volume voxels/cubes. The values, given below the shapes, relate to the estimated fitting cylinders (h_l and h_s), the computed quantities $\mathcal{C}_1$ and $\mathcal{C}_2$, and finally to the computed cylinderness measures $\mathcal{C}$.

with small exception for nearly spherical $3D$ shapes. If the method is applied to the $3D$ voxelized shapes it has an asymptotically optimal time complexity – i.e. it has the $\mathcal{O}(N)$ computational complexity, where N is the number of voxels that belong to the digitized shape considered.

Further, the fitting cylinders obtained are used to design a new $3D$ shapes measure. This measure is named a *cylinderness measure*, since it gives a numerical evaluation of how much a $3D$ shape given looks like a perfect cylinder. The new measure has the following desirable properties: **(i)** It varies through the interval $[0, 1]$; **(ii)** The measure picks the value 1 if and only if the shape measured is a cylinder; **(iii)** The measure is invariant with respect to the translation, rotation, and scaling transformations. Being theoretically well founded, the behavior of the new measure can be predicted to some extent, without verification experiments needed. This is always an advantage.

The initial method (described in Definition 2 and Definition 3) requires the incremental rotations of the shape measured (see the role of the parameter α in Definition 2), for the computation of the cylinderness measure. In order to avoid the required incremental rotations of the shape considered, a modified method for the computation of the shape cylinders measure is introduced (see Definition 4 and Definition 5). The modified method uses principal axes, for the $3D$ shape cylinderness computation. In this way incremental rotations are not needed. The fitting cylinders are the same in initial method and its modification.

Notice that the computation of fitting cylinders, for a given shape S, is a *shape based* one since it is based on the (shape moments) invariant $J(S)$. The invariant $J(S)$ is computable from low-order moments, i.e. the moments whose order is upper bounded by two. Such a selection is made to simplify the computation of the fitting cylinder parameters. The cylinderness measure established uses a standard geometric approach, where the set difference between the shape considered and its fitting cylinders is observed.

Several experiments on synthetic data/shapes and the shapes selected from the well-known McGill 3D Shape Benchmark data set [20] are provided. The cylinders measure values obtained may be understood as reasonable and expected ones.

Experiments on shapes subjected to deformation transforms, and eroded discretized shapes are also provided. These show that the new measure is robust.

Despite the fact that all theoretical derivations and observations are made in a continuous space, the new cylinderness measure is aimed to be applied to the computer manipulated $3D$ images, or more generally $3D$ point sets. Thus, all the experiments are performed on discrete point sets, obtained in a process of the voxelization of real objects. This always implies an inherent computation error. A good thing here is that the measure is applied to the solid $3D$ shapes – i.e. all the shape points are taken into account, not only the boundary ones, for example. This further implies that all the parameters (the $3D$ moment invariant used, and volumes of the shapes considered), needed for the computation of the cylinderness measure $\mathcal{C}(S)$, can be computed efficiently (within a small approximation error), as it is well known [4, 11] from the number theory.

7 Acknowledgment

The authors wish to hank to Dr. Carlos Martinez-Ortiz for his help during the preparation of this paper.

This work is partially supported by the Serbian Ministry of Science and Technology.

References

[1] Aktaş, M.A., Žunić, J.: 'A family of shape ellipticity measures for galaxy classification,' *SIAM Journal on Imaging Sciences*, (2013) **6**, pp. 765–781.

[2] Aylward, S., Jomier, J., Weeks, S., Bullitt, E.: 'Registration and analysis of vascular images,' *International Journal of Computer Vision,* (2003) **55**, pp. 123–138.

[3] Chambers, C.P., Miller, A.D.: 'A measure of bizarreness,' *Quarterly Journal of Political Science,* (2010) **5**, pp. 27–44.

[4] Davenport, H.: 'On a principle of Lipschitz,' *J. London Math. Soc.,* (1951) **26**, pp. 179–183.

[5] Duda, R.O, Hart, P.E., Stork, D.G.: *Pattern classification* (2nd Edition), Wiley, New York, 2001.

[6] Dupain, Y., Kamae, T., Mendés, M.: 'Can one measure the temperature of a curve?' *Archive for Rational Mechanics and Analysis,* (1986) **94**, pp. 155–163.

[7] Edelsbrunner, H., Pausinger, F.: 'Stable length estimates of tube-like shapes,' *J. Math. Imaging Vis.,* (2013) **50**, 164–177.

[8] Frangi, A.F., Niessen, W.J., Vincken, K.L., Viergever, M.A.: 'Multiscale vessel enhancement filtering,' MICCAI'98, (1998) *LNCS*, **1496**, pp. 130–137.

[9] Gabrielides, C.N., Sapidis, N.S: 'Shape analysis of generalized cubic curves,' *Computer-Aided Design,* (2020) **125**, article no. 102849

[10] Genctav, A., Tari, S.: 'Discrepancy: Local/global shape characterization with a roundness bias' *J. Math. Imaging Vis.*, (2019) **61**, pp. 160–171.

[11] Huxley, M.N., Klette, R., Žunić, J.: *Precision of Geometric Moments in Picture Analysis,* chapter in Geometric Properties from Incomplete Data, editors: R. Klette, R. Kozera, L. Noakes, J. Weickert, pp. 221–235, Kluwer Publisher, 2006.

[12] Hu, M.: 'Visual pattern recognition by moment invariants,' *IRE Trans. Information Theory*, (1961) **8**, pp. 179–187.

[13] Lain Z., Rosin P.L., Sun X.: 'Rectilinearity of 3D meshes.' *Int. J. Comput. Vis.,* (2010) **89**, pp. 130–151.

[14] Lo, C.-H., Don, H.-S.: '3-D moment forms: their construction and application to object identification and positioning', *IEEE Trans. Pattern Analysis Machine Intelligence,* (1989) **11**, pp. 1053–1064.

[15] Ma, Z., Ma, J., Xiao, B., Lu, K.: 'A 3D polar-radius-moment invariant as a shape circularity measure,' *Neurocomputing,* (2017) **259**, pp. 140–145.

[16] Mamistvalov, A.G.: 'n-Dimensional moment invariants and conceptual mathematical theory of recognition n-dimensional solids,' *IEEE Trans. Pattern Analysis Machine Intelligence,* (1998) **20**, pp. 819–831.

[17] Marshall, D., Lukacs, G., Martin, R.: 'Robust segmentation of primitives from range data in the presence of geometric degeneracy,' *IEEE Trans. Pattern Analysis Machine Intelligence,* (2001) **23**, pp. 304–314.

[18] Martinez-Ortiz, C., Everson, R.: 'Minkowski compactness measure,' 13^{th} UK Workshop on Computational Intelligence – UKCI, (2013) pp. 62–66.

[19] Martinez-Ortiz, C., Žunić, J.: 'A family of cubeness measures,' *Machine Vision and Applications,* (2012) **23**, pp. 751–760.

[20] McGill 3D Shape Benchmark data set:
http://www.cim.mcgill.ca/∼shape/benchMark/

[21] Misztal, K., Tabor, J.: 'Ellipticity and circularity measuring via Kullback–Leibler divergence,' *J. Math. Imaging Vis.,* (2016) **55**, pp. 136–150.

[22] Nievergelt, Y.: 'Fitting cylinders to data,' *Journal of Computational and Applied Mathematics,* (2013) **239**, pp. 250–269.

[23] Nurunnabi, A., Sadahiro, Y., Lindenbergh, R., Belton, D.: 'Robust cylinder fitting in laser scanning point cloud data,' *Measurement,* (2019) **138**, pp. 632–651

[24] Proffitt, D.: 'The measurement of circularity and ellipticity on a digital grid,' *Pattern Recognition,* (1982) **15**, pp. 383–387.

[25] Rhouma, M.B.H., Žunić, J., Younis, M.C.: 'Moment invariants for multi-component shapes with applications to leaf classification,' *Computers and Electronics in Agriculture,* (2017) **142**, pp. 326-337.

[26] Rosin, P.L., Pantović, J., Žunić, J.: 'Measuring linearity of curves in 2D and 3D,' *Pattern Recognition,* (2016) **49**, pp. 65–78.

[27] Rosin, P.L., Žunić, J.: 'Measuring squareness and orientation of shapes,' *J. Math. Imaging Vis.,* (2011) **39**, pp. 13–27.

[28] Sadjadi, F.A., Hall, E.L.: 'Three-dimensional moment invariants', *IEEE Trans. Pattern Analysis Machine Intelligence,* (1980) **2**, pp. 127–136.

[29] Tool, A.Q.: 'A method for measuring ellipticity and the determination of optical constants of metals', *Phys. Rev. (Series I),* (1910) **31**, pp. 1–25.

[30] Tran, T.-T., Cao, V.-T., Laurendeau, D.: 'Extraction of cylinders and estimation of their parameters from point clouds,' *Computers & Graphics,* (2015) **46**, 345–357.

[31] Xu, D., Li, H.: 'Geometric moment invariants,' *Pattern Recognition,* (2008) **41**, pp. 240–249.

[32] Zhang, Z., Li, J., Guo, Y., Li, X., Lin, Y., Xiao, G., Wang, C.: 'Robust procedural model fitting with a new geometric similarity estimator,' *Pattern Recognition,* (2019) **85**, 120–131.

[33] Žunić, A.: 'Shape diameter for object analysis,' *Inf. Process. Lett.,* (2018) **136**, pp. 76–79.

[34] Žunić, J., Hirota, K., Rosin, P.L.: 'A Hu invariant as a shape circularity measure,' *Pattern Recognition,* (2010) **43**, pp. 47–57.

[35] Žunić, J., Hirota, K., Dukić, D., Aktas, M.A.: 'On a 3D analogue of the first Hu moment invariant and a family of shape ellipsoidness measures,' *Mach. Vis. Appl.,* (2016) **27**, pp. 129–144.

[36] Žunić, J., Hirota, K., Martinez-Ortiz, C.: 'Compactness measure for 3D shapes,' Proc. IEEE/IAPR ICIEV 2012 Conference, Dhaka (Bangladesh), (2012) pp. 1180–1184.

[37] Žunić, J., Stojmenović, M.: 'Boundary based shape orientation', *P*attern Recognition, (2008) **4**1, pp. 1768-1781.

[38] Žunić, J., Žunić, D.: 'Shape interpretation of second order moment invariants,' *J. Math. Imaging Vis.*, (2016) **56**, 125–136.